NMR measurements on ³He adsorbed on Grafoil at submonolayer coverages and millikelvin temperatures

K.-D. Morhard, J. Bossy, and H. Godfrin

Centre de Recherches sur les Très Basses Températures, Centre National de la Recherche Scientifique,
Boîte Postale 166, 38042 Grenoble CEDEX 9, France

Precise nuclear magnetic susceptibility results on ³He adsorbed on Grafoil are presented for submonolayer coverages in the temperature range 5–600 mK. At low areal densities, the film is in a two-dimensional homogeneous liquid state. Some ³He atoms, however, are localized by the substrate heterogeneity; our quantitative measurements show that their amount increases from 2% to 4% of a monolayer thereby leading to significant corrections of the fluid-phase density. The Fermi temperature of the liquid has been determined as a function of coverage; it decreases continuously for densities larger than 0.01 atoms/Å². At high fluid densities, the susceptibility is enhanced by one order of magnitude with respect to the ideal-gas value. At $\rho = 0.0449$ atoms/Å², a two-phase coexistence region begins on a Grafoil sample; $\rho = 0.0434$ atoms/Å² is estimated for a perfect graphite surface. The coexistence is characterized by a linear increase (linear decrease) of the solid (liquid) fraction and a constant Fermi temperature of the liquid phase. Finally, at $\rho = 0.0646$ atoms/Å², the liquid phase disappears completely. Our results are compared to previous heat capacity and NMR measurements at submonolayer coverages.

I. INTRODUCTION

Currently there is considerable interest in the structural and magnetic properties of ³He films adsorbed on Grafoil,[1] an exfoliated graphite characterized by a large specific area. Recent work has shown that ³He films adsorbed on graphite are simple experimental model systems particularly suited for theoretical calculations and computer simulations, providing canonical examples of two-dimensional (2D) Fermi liquids and quantum solids. The phase diagrams of the first and of the second layer have been studied by NMR and heat capacity techniques, leading to the observation of two-dimensional nuclear antiferromagnetism and ferromagnetism. A review of this subject is given in Refs. 2–5.

The first layer of ³He on Grafoil, which represents the simplest of the systems mentioned above, displays a variety of structural phases. At very low surface densities, all adsorbed atoms are localized by substrate heterogeneities, building up immobile patches of high-density solid. At higher surface densities, a 2D fluid phase of increasing density is observed until the system enters a fluid-solid coexistence region where the solid phase consists of the commensurate √3 phase. The density of the pure commensurate phase is $\rho = 0.063\,66$ atoms/Å², as calculated from the graphite lattice parameter. By increasing the density still further, the system evolves from the commensurate solid to several other phases, then forms an incommensurate solid, and finally promotion of atoms into the second layer occurs.

Although, at first sight, this phase diagram seems to be rather well established, there remain several open questions, especially when analyzing data with high precision. Several physical properties depend crucially on the accuracy of the measured densities: for instance, the density dependence of the effective mass, the existence of vacancy commensurate solids, commensurability effects in multilayer films, etc. Unfortunately, since the existence of localized atoms at low densities is not detected by heat capacity measurements at low temperatures, the densities reported in heat capacity work are less accurate than usually believed. Finally, there is a serious discrepancy between heat capacity[6] and previous NMR data[7] on the onset of the coexistence region mentioned above.

It is the aim of this work to clarify the questions related to heterogeneity and to the transition to the commensurate phase as well as to investigate in detail the properties of submonolayer liquid ³He.

II. EXPERIMENTAL DETAILS

A general discussion of the surface physics techniques developed in our laboratory to study adsorbed ³He at millikelvin temperatures can be found in a recent publication.[8]

The dilution refrigerator used in the present experiment reaches a minimum temperature of less than 3 mK at a flow rate of 140 μmol/s. With the whole experimental setup mounted, this minimum temperature increases to about 3.3 mK. Contrarily to the experiment described in Ref. 8, here the experimental cell is located outside the mixing chamber as shown in Fig. 1. This construction suppresses the background signal from the ³He in the
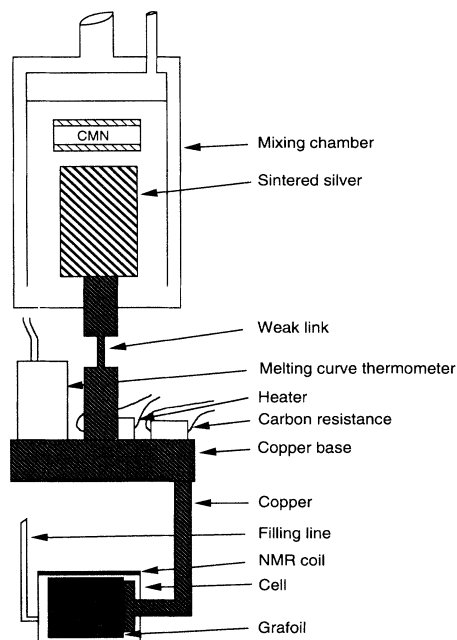
FIG. 1. Experimental setup.

mixing chamber at the cost of a reduced thermal shielding. The graphite sample consists of a stack of Grafoil[1] plates bonded on both sides to thin copper foils in order to ensure a good thermal contact. Therefore 26 Grafoil plates of length 2.3 cm and thickness 0.4 mm were bonded to 13 copper foils, each stack being separated from the next one by cigarette paper. The assembly is of cylindrical overall shape and fits inside a 1.5 cm diameter plastic cell. The copper foils are welded to a copper post that passes through the cell's end cover, ensuring thermal contact to a copper base by means of a copper wire. The copper base is thermally coupled to a silver heat exchanger located inside the mixing chamber through a calibrated thermal resistance with $R_{th} = 400/T \, (\mathrm{K}^2/\mathrm{W})$. The copper base is mechanically attached to the body of the plastic mixing chamber by three Vespel rods. A 1.2 mm inner diameter filling capillary is connected to the cell through a 2.5 cm length, 1 mm inner diameter Araldite tube. The diameter of the capillary increases at the higher-temperature locations inside the cryostat, up to 2.5 mm at room temperature, where it is connected to the gas handling system. The NMR coil is wound on the body of the plastic sample cell. It consists of 211 turns of 0.04 mm diameter copper wire; its diameter is 1.95 cm and its length 2.4 cm. Its inductance was measured to be 0.46 mH. Electrical connections to the coaxial line are made with Niomax 065CN superconducting wire.

The temperature was determined by a ³He melting-curve thermometer located on the copper base (see Fig. 1). The design is similar to Greywall and Busch's,[9] but the performance was optimized to give a lower noise and an improved stability against thermal cycling. Further details will be given in a forthcoming publication. A

carbon resistance (Speer 100 Ω), appropriately filtered against electrical interference, was also used as thermometer in the temperature range above 10 mK. It was calibrated against the ³He melting-curve thermometer at low temperatures and against a CMN thermometer placed in the mixing chamber. The temperature regulation of the copper base was ensured by the temperature controller of the capacitance bridge associated to the melting-curve thermometer, or by that of the resistance bridge, depending on the temperature range.

At the lowest temperatures, we observed a temperature gradient between the copper base and the experimental cell. This was deduced from a deviation of the susceptibility from a Curie law for an adsorbed ³He sample at a coverage $\rho = 0.0908$ atoms/Å² where previous data[8] exclude any substantial departures from a Curie law. The measured susceptibility could be well described by a model assuming a constant heat leak. All sample temperatures given in this work have been corrected for this effect. This correction is only important at low temperatures; in particular, the minimum sample temperature in this work was 4.8 mK. The source of the heat leak could be attributed to a faulty thermal anchoring of the coaxial line of the NMR coil onto the copper base. This was verified by a complementary measurement at the coverage $\rho_0 = 0.0908$ atoms/Å²; improving the thermal ground caused a reduction of the heat leak to a nonmeasurable level.

To determine the surface area of our Grafoil sample we made an adsorption isotherm at 4.2 K (Fig. 2). Bretz et al.[10] give the adsorbed volume at perfect registry (areal density $\rho_0 = 0.063\,66$ atoms/Å²) and an adsorption isotherm at 4.2 K measured on the same Grafoil sample. By scaling the two isotherms, we determine the surface area of our cell to be $A_c = 46.87$ m². This area determination based on the commensurate phase defines the "commensurate coverage scale"[8] for our sample.

The samples were prepared by introducing known amounts of ³He gas into the experimental cell at 4.2 K. The cell was then heated to 8 K for several hours (typically overnight) to anneal the ³He film. Great care was
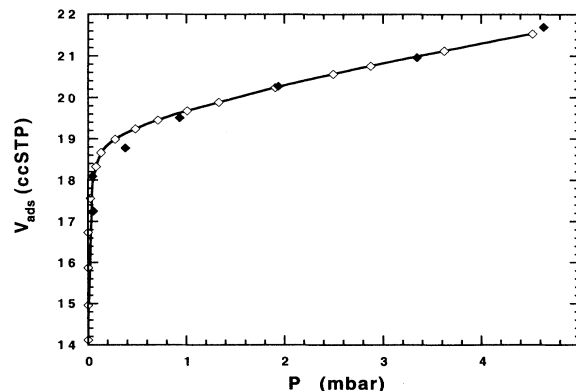
FIG. 2. ³He adsorption isotherm at 4.2 K; open squares, our data; solid squares, data of Bretz et al. (Ref. 10) scaled to superpose our data.

taken to lower the temperature sufficiently slowly in order to ensure thermodynamic equilibrium.

The NMR signal was measured with a continuous wave spectrometer operating at a frequency of 470.6 kHz corresponding to a magnetic field of 14.5 mT. The maximum voltages on the rf coil were limited by heating of the Grafoil sample and typically ranged from 2 to 10 mV. The absorption signal on the coil was about 1 μV at coverages below 0.4 layers and at 5 mK. The area under the NMR absorption signal was determined by numerical integration of the NMR line. It is important to ensure that the whole NMR line is covered by the field sweep. This is done by determining the minimum field sweep leading to less than 2% loss of area for each coverage. This sweep amplitude was found to be around 8 G in all our coverages and corresponds to about 30 times the linewidth. The number of NMR lines taken for averaging ranged from 30 to 150 lines depending on temperature and was limited by the systematic error becoming larger than the statistical error at that number. It has to be stressed that the susceptibility is determined by numerically integrating the NMR signal and not by fitting a Lorentzian. Theoretically, the statistical error bars could be reduced by using the second method, but at the cost of possible systematic errors in the case of the NMR line not following a Lorentzian behavior.
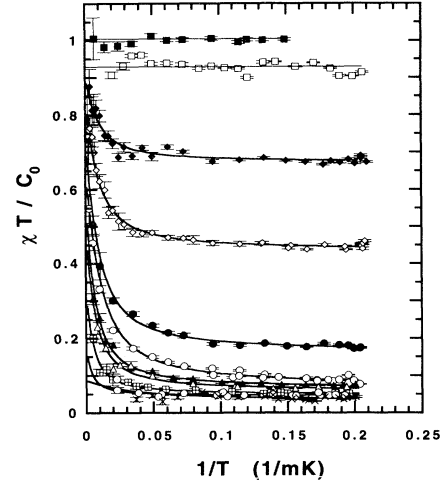

FIG. 3. Normalized susceptibility $\chi T/C_0$ as a function of the inverse temperature; C_0 is the Curie constant of the commensurate phase; crosses, 0.0055; dotted circles, 0.0107; crossed squares, 0.0207; open triangles, 0.0307; solid triangles, 0.0358; open circles, 0.0411; solid circles, 0.0467; open diamonds, 0.0523; solid diamonds, 0.0571; open squares, 0.0625; and solid squares, 0.0646 atoms/Å^2.

III. EXPERIMENTAL RESULTS

The nuclear susceptibility of adsorbed ^{3}He has been measured at 12 coverages (ρ = 0.0055, 0.0107, 0.0207, 0.0307, 0.0358, 0.0411, 0.0467, 0.0523, 0.0571, 0.0625, and 0.0646 atoms/Å^2 as well as ρ = 0.0908 atoms/Å^2 for calibration purposes) at temperatures between 4.8 and 600 mK. The nuclear susceptibility χ is proportional to the area under the NMR absorption signal.[11] The Curie constant C_ρ is proportional to the number of spins, and hence to the areal density ρ. In this coverage range, it is convenient to use the Curie constant C_0 at the commensurate phase density ρ_0 as a reference:

$$C_\rho = C_0 \, \frac{\rho}{\rho_0},$$

where ρ_0 = 0.063 66 atoms/Å^2. We determine C_0 by a calibration run at a coverage of 0.0908 atoms/Å^2 corresponding to a solid incommensurate phase where previous experiments showed that there are no substantial departures from a Curie law.

At the low coverages studied here, the system is expected to consist of both liquid and solid phases. Due to the degeneracy of the liquid for temperatures below the Fermi temperature (found to be at about 200 mK), the measured total susceptibility is dominated by the large Curie contribution of the solid. At temperatures larger than the Fermi temperature, the spins of both phases follow a Curie law. It is therefore convenient to show the experimental results in a plot of $\chi T/C_0$ vs $1/T$ in order to emphasize departures from Curie behavior; this plot can be seen in Fig. 3. The high-temperature limiting value

of $\chi T/C_0$ is proportional to the amount of adsorbed helium. At temperatures below about 40 mK, a strongly coverage dependent Curie contribution, corresponding to the solid phase, is found. The liquid contribution is also clearly seen in Fig. 3: It corresponds to the rapid decrease of $\chi T/C_0$ as a function of $1/T$ due to the onset of degeneracy. The error bars correspond to the statistical error determined from the measurement of several NMR lines. The 1 σ error bars represent adequately the experimental uncertainty for small signals, as observed at low coverages or high temperatures. On the other hand, the uncertainty of large signals, corresponding to high coverages and low temperatures, is clearly dominated by systematic errors; in this case the dispersion of the data (see Fig. 3) is mainly due to low-frequency instabilities of the NMR base line. The magnitude of the systematic errors is obviously deduced from the scatter in the data.

The data for areal densities below 0.0625 atoms/Å^2 were fitted by the expression

$$\frac{\chi T}{C_0} = n_{\text{solid}} + \frac{n_{\text{liquid}} \, T}{T_F^{**}} \left(1 - e^{-T_F^{**}/T}\right),$$

where $n_{\text{solid}} = N_{\text{solid}}/N_0$ and $n_{\text{liquid}} = N_{\text{liquid}}/N_0$; N_{solid}, N_{liquid}, and N_0 are the number of atoms in the solid, liquid, and the pure commensurate phases, respectively. The expression given above corresponds to N_{solid} atoms following a Curie law and therefore being in a solid phase and N_{liquid} atoms in a liquid phase with an effective Fermi temperature T_F^{**}.[7,12] Since $n_{\text{solid}} + n_{\text{liquid}} = N/N_0 = \rho/\rho_0$, there are only two adjustable parameters n_{solid} and T_F^{**}. This very simple formula provides a good fit of the experimental data in all the temperature and coverage

range investigated here.

The coverage dependence of the solid part of the ³He film, n_{solid}, is shown in Fig. 4. At low densities, there is a small amount of solid growing linearly from 2% of a monolayer to about 4% at 0.04 atoms/Å². Between 0.0467 atoms/Å² and 0.0571 atoms/Å², the amount of solid increases linearly with coverage, indicating a two-phase coexistence between solid and liquid. A linear extrapolation to the diagonal line where $n_{solid} = N/N_0$ (corresponding to all of the atoms being in the solid phase) gives an areal density of 0.0641 atoms/Å², thereby confirming the assumption that the solid exists in the commensurate phase. The onset of the coexistence region can be characterized, as will be discussed later on, either by an extrapolation to $n_{solid} = 0$ (point a at 0.0434 atoms/Å²) or by the intercept of the two straight lines shown in Fig. 4 (point b at 0.0449 atoms/Å²). At a density of 0.0646 atoms/Å², the film has completely solidified and $n_{solid} = 1$.

The coverage dependence of the Fermi temperature of the liquid fraction is shown in Fig. 5. The Fermi temperature of an ideal 2D Fermi gas is given by the expression

$$T_F = \frac{\pi \, \hbar^2 \, N}{k_B \, m_3 \, A},$$

where N is the number of atoms and A is the total surface area. Using the numerical values of the physical constants, this gives

$$T_F \, [\mathrm{K}] = 50.53\rho \, [\mathrm{atoms/Å}^2].$$

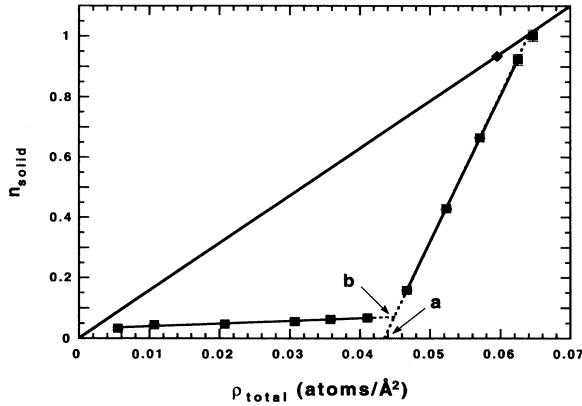This function is shown by the solid line in Fig. 5. Note that this line has been shifted in coverage by 2% of a
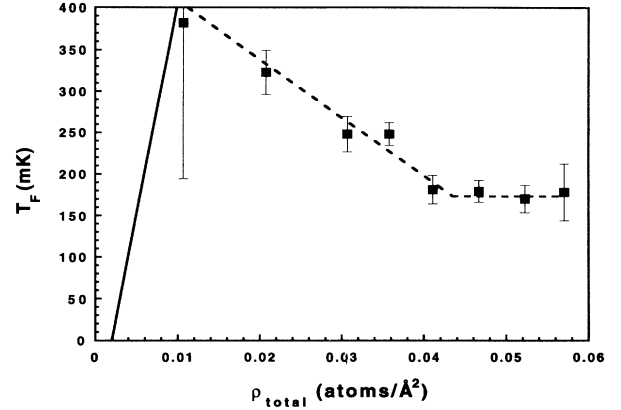

FIG. 5. Fermi temperature T_F^{**} as function of the areal density; the solid line corresponds to ideal-gas behavior, shifted to take into account the heterogeneity effects (see text); the dotted line is a guide to the eye.

monolayer, thereby taking into account the ³He atoms localized at surface heterogeneities. Due to the extremely small susceptibility signal at the lowest coverage, it was not possible to determine the Fermi temperature of the film at this coverage with precision; values between 50 and 400 mK are consistent with our data. For the lowest two coverages, the experimental data are in reasonable agreement with the Fermi gas expression. At higher coverages, the Fermi temperature is found to decrease substantially and then to reach a plateau for coverages in the solid-liquid coexistence region.

In Fig. 6 a plot of the total susceptibility as a function of the inverse temperature is shown for $\rho = 0.0523$ atoms/Å², a selected coverage where the solid and liquid fractions are comparable. Also shown is the susceptibility of the Fermi liquid only; the solid part of the signal
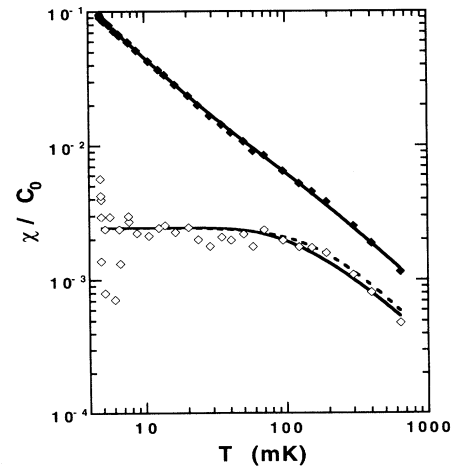

FIG. 4. Density dependence of the solid fraction $n_{solid} = N_{solid}/N_0$ where N_{solid} is the number of atoms in solid phases and N_0 that at the commensurate phase; the diagonal line corresponds to $n_{solid} = \rho/\rho_0$ where ρ_0 is the commensurate phase density; the dotted lines are extrapolations of the linear region at low densities and the linear coexistence region, respectively; the solid diamond corresponds to the value expected for a solid containing 6% of vacancies as proposed by Greywall and Busch (Ref. 6); points a and b denote the onset of the commensurate phase formation for a perfect graphite and a Grafoil sample, respectively.

FIG. 6. χ/C_0 as a function of the temperature for $\rho = 0.0523$ atoms/Å²; solid diamonds, total susceptibility; open diamonds, susceptibility of the Fermi liquid (the solid contribution has been subtracted); fits as explained in the text.

has been subtracted. For high temperatures the signal of the liquid decreases following a Curie law, whereas at low temperatures the susceptibility reaches a limiting value. The fit to the liquid susceptibility (corresponding to the solid line in Fig. 6) was done with the equation

$$\frac{\chi}{C_0} = \frac{1}{T_F^{**}} (1 - e^{-T_F^{**}/T}),$$

whereas the fit corresponding to the hatched line was done with the expression proposed by Dyugaev:[13]

$$\frac{\chi}{C_0} = \frac{1}{\sqrt{T^2 + T_F^{**\, 2}}}.$$

The difference in the Fermi temperatures determined by the fits with both formulas was inside the error bars for all coverages. In both cases there was only one fit parameter T_F^{**}. It should be pointed out that the Fermi temperatures obtained using only the data in the degenerate regime coincide with those using the full temperature dependence. Within our present accuracy the values of the Fermi temperatures deduced from the low-temperature limiting susceptibility are the same as the characteristic degeneracy temperatures; note, however, that some difference between these two characteristic temperatures has been observed in second layer fluids in preplated systems;[5] we also have evidence for the same behavior in the second layer of pure ^{3}He films. Clearly, this subject deserves further investigation.

IV. DISCUSSION

The small Curie-like signal at surface densities below the solid-liquid coexistence region is due to atoms localized by heterogeneities in the Grafoil substrate. We find for the amount of this solid a value of $n_{\text{solid}} = 0.0324$ at the lowest density. This value increases linearly to 0.0628, at a density just below the onset of the coexistence region. Early heat capacity measurements on low-density samples[10] already showed the existence of localized atoms, forming patches at large binding energy sites. A theoretical approach is due to Elgin et al.,[14] who proposed a model based on a distribution of binding energies associated to defects of the graphite surface (corners where graphite platelets join). A characteristic coverage of 0.0023 atoms/Å^2 was found.[15] This was verified by pulsed NMR measurements,[16] deducing from T_2 data that 0.005 of a monolayer are strongly localized, whereas 0.015 of a monolayer are immobile. Note that this measurement is performed at the relatively high temperature of 1.2 K. Measurements by cw NMR techniques at lower temperatures[7] indicate that the solid fraction corresponds to 0.0022 atoms/Å^2. Our data agree with the magnitude reported for this effect; in addition they clearly show an increase of the solid fraction as a function of total coverage. This behavior is precisely that expected for a distribution of binding energies, as proposed by Elgin and Goodstein.[14]

It must be pointed out that a substantial fraction of a monolayer (about 4%) may be affected by heterogeneity; this figure is not negligible when analyzing adsorbed ^{3}He data.

The beginning of the formation of commensurate solid is determined by the present measurement to be at the point b of Fig. 4 (0.0449 atoms/Å^2). Note that the effect of heterogeneities is to overestimate the areal density at the onset. Its value for a perfect graphite substrate can be estimated from point a in Fig. 4 to 0.0434 atoms/Å^2. Our onset value at the point b is slightly higher than that given by heat capacity measurements[6] where an onset value of 0.043 atoms/Å^2 is found. The 4% discrepancy might be considered as being within the combined error bars in the absolute coverage scale; see, however, the discussion on this point given below. A more serious discrepancy is found when comparing these figures to that found in previous low-temperature NMR measurements,[7] where the liquid-commensurate phase coexistence is reported to start at a density as low as 0.032 atoms/Å^2. Note that completion of the commensurate phase is found in all experiments at the expected coverage (around 0.063 66 atoms/Å^2). Therefore, the discrepancy can not be attributed to a proportional shift of the coverage scales. The most likely explanation is that proposed by Greywall and Busch,[6] stating that inadequate annealing in the experiment reported in Ref. 7 could have caused an inhomogeneous distribution of the adsorbed ^{3}He atoms. Dramatic annealing effects on the heat capacity have been reported in the literature,[6,10] but, to our knowledge, no systematic investigation has been performed. The effects of annealing of submonolayer films is still a rather open problem.

The completion of the commensurate phase is a particularly interesting problem. It has been pointed out by Greywall and Busch[6] that total solidification may occur at coverages slightly lower than that corresponding to perfect registry. Heat capacity data suggest that an unusual solid containing as much as 6% of vacancies could be formed, this amount being reduced as perfect registry is approached. Our data do not support this contention. As seen in Fig. 4, we observe that a total solidification of the ^{3}He film is achieved at a coverage 0.0646 atoms/Å^2, practically coincident with the pure commensurate coverage. In Fig. 4 the point where full solidification into a vacancy solid was expected from heat capacity data is indicated. The discrepancy is obvious. It should be pointed out, however, that an alternative explanation for the heat capacity was already proposed by Greywall and Busch.[6] Assuming a different coverage scale, consisting basically in determining the commensurate phase coverage as that where the amount of liquid extrapolates to zero (instead of that corresponding to the actual minimum of the heat capacity isotherms), Greywall and Busch conclude that heterogeneity may explain the liquidlike signal now found above perfect commensurability. Note that the heterogeneity in this case corresponds to regions of less attractive potential. Under this assumption Greywall and Busch's original coverage scale is modified by about 4%. This corrected coverage scale is in agreement with the one used in the present work: The onset of the coexistence is now found at exactly the same coverage, and

excellent agreement is found for the total solidification coverage. In addition, in our work the commensurate coverage is defined as that having the highest melting temperature since our coverage scale is based on that obtained by Bretz et al.[10] We find therefore that complete solidification coincides with the highest melting temperature. It would be surprising that a vacancy solid phase would have a higher melting temperature than the completed commensurate phase. From this we deduce that the most likely explanation for the anomalous behavior observed by Greywall and Busch is a progressive solidification of fluid at heterogeneous sites above the commensurate phase coverage. The existence of a vacancy solid seems therefore questionable. A measurement of the heat capacity in a large temperature range (including melting), and also of the magnetic susceptibility, should be performed on the same sample to solve this problem unambiguously. Supporting the preceding conclusions is the remarkable absence of any substantial deviations of the susceptibility from a Curie law for all the coverages investigated here (Curie-Weiss temperatures are found to be smaller than 0.2 mK). That is, we find no evidence for the vacancy induced ferromagnetism predicted by Guyer[17] which could be expected if the solid contained 6% of vacancies.

The properties of two-dimensional liquid ³He films have attracted some interest in recent years. Heat capacity measurements[10,18] allowed the observation of Fermi-liquid behavior in submonolayer ³He films. Fermi temperatures on the order of 200 mK are obtained from these measurements. More accurate values were obtained by recent NMR measurements,[7] the first ones to investigate the fully degenerate regime. Values of the Fermi temperature in the range 150–300 mK were found. The precision of our data, however, allows one to infer the coverage dependence of the effective Fermi temperature T_F^{**} of submonolayer ³He films (see Fig. 5). For coverages larger than 0.01 atoms/Å², T_F^{**} decreases progressively, a behavior similar to that observed in bulk liquid ³He as the pressure (and hence the density) is increased. A similar feature is observed qualitatively in the heat capacity results.[10] Our data display another feature compared to previous NMR results. As seen in Fig. 5, T_F^{**} remains constant in the liquid-solid coexistence regime, as could be expected from a simple coexistence model with a commensurate solid of constant density which is imposed by the substrate.

The Fermi-liquid properties of submonolayer ³He can be studied in a large density range, up to 0.0435 atoms/Å². Therefore they are of particular interest from the point of view of the theory of Fermi liquids. The susceptibility enhancement, defined as the susceptibility of an interacting Fermi liquid at zero temperature $\chi(0)$ divided by the ideal Fermi-gas value $\chi_0(0)$, is given by

$$\frac{\chi(0)}{\chi_0(0)} = \frac{T_F}{T_F^{**}}.$$

A plot of this enhancement factor as a function of the density of the liquid is shown in Fig. 7 for total surface densities below the onset of the coexistence region. Note
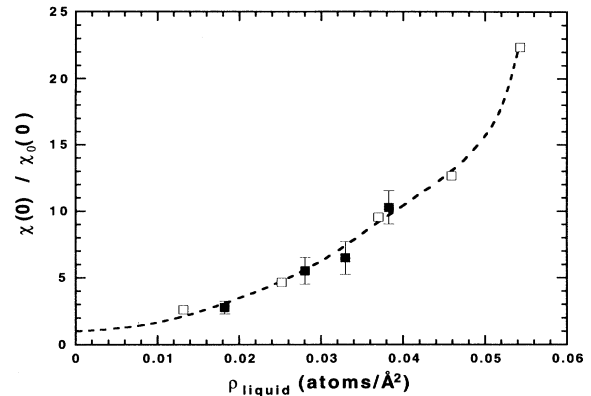

FIG. 7. Susceptibility enhancement as a function of the liquid density for the first and second layers respectively; solid diamonds, first layer (this work); open diamonds, second layer with a first layer of ⁴He [Lusher et al. (Ref. 19)]; the hatched line serves as a guide to the eye.

that the contribution of the localized atoms has been subtracted from the total density to obtain the true liquid density; the microscopic density of the solid was taken to be 0.11 atoms/Å² (that of a compressed monolayer), in order to calculate the area available to the liquid. It is interesting to compare these results to those obtained by Lusher and co-workers on a related system:[19] fluid ³He on top of a monolayer of ⁴He on a graphite substrate. In this case, the adsorption potential is much weaker with a binding energy of a few tens of Kelvin, compared to 136 K for bare graphite. In addition, the corrugation of the substrate potential is strongly reduced. Comparing both systems should, a priori, provide a test of the influence of the delocalization along the direction normal to the adsorption plane. A comparison of our submonolayer data with those on the preplated system is given in Fig. 7. The coverage range that can be explored on the preplated system is larger than that available on bare graphite, since, on the latter, the commensurate phase is more stable than a high-density fluid. Nevertheless, at the maximum fluid density investigated here, enhancement factors as high as 10 were observed. It is remarkable that, within error bars of similar magnitude, the enhancement factors measured for both systems have the same dependence on the liquid density.

The enhancement factor is related to the Landau parameter F_0^a by the equation

$$\frac{\chi(0)}{\chi_0(0)} = \frac{m^*}{m} \frac{1}{1 + F_0^a}.$$

The Landau parameter can be determined by taking effective mass values from heat capacity measurements. The effective mass at submonolayer coverages has been determined by McLean[20] and more recently by Greywall and Busch[21] (Fig. 8) as a function of the total density. According to our data, however, the density of the liquid is significantly lower than the total density due to the amount of localized ³He. Correcting for this effect leads
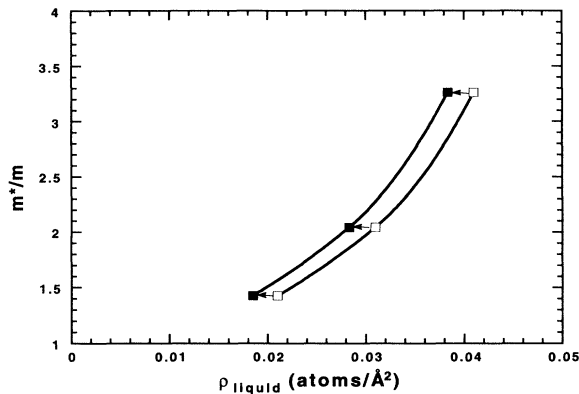
FIG. 8. Effective mass of the first layer as a function of first layer liquid density determined using the heat capacity data by Greywall and Busch (Ref. 21); open squares, first layer ^{3}He before correction for the localized atoms (see text); solid squares, first layer ^{3}He after correction.

to a substantial modification of the coverage dependence of the effective mass of the submonolayer liquid as indicated in Fig. 8.

The Landau parameter F_0^a deduced from the equation above, where the effective mass is taken from Fig. 8 (using the corrected coverage scale), is shown in Fig. 9 plotted as a function of the inverse of the effective mass. Also shown in Fig. 9 are the values from ^{3}He in the second layer[19] as well as bulk ^{3}He data.[22] Note that the second layer data correspond to ^{3}He on top of a ^{4}He monolayer
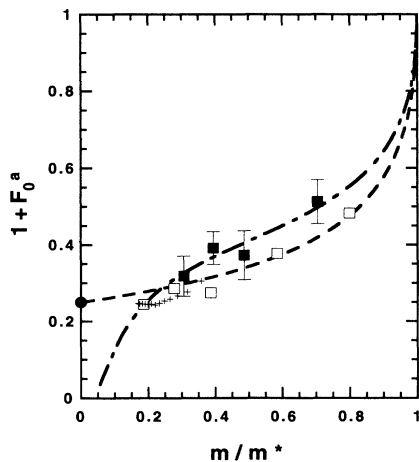

FIG. 9. Landau parameter $1 + F_0^a$ as a function of m/m^*; solid squares, first layer ^{3}He [susceptibility data, this work; heat capacity, Greywall and Busch (Ref. 21)]; open squares, susceptibility data on second layer ^{3}He with a first layer of ^{4}He [Lusher et al. (Ref. 19)] and heat capacity data on pure ^{3}He films (Ref. 21) (for the analysis a similar behavior for both systems has to be assumed); crosses, bulk ^{3}He (Ref. 22); hatched line, almost localized fermion theory (see text); point-hatched line, paramagnon model (see text); solid circle, value from "spin-glass" model by Castaing (Ref. 30).

that were analyzed using the values of the effective mass reported by Greywall and Busch for a different system (pure ^{3}He films[23]). In addition, the second layer density is not known accurately for the latter system, since the compression of the first layer as measured by neutron scattering[24] is not taken into account. In fact, this effect should shift the values of the effective mass to lower densities except very close to second layer promotion. It is difficult to evaluate precisely the systematic errors for the case of the second layer data of Ref. 7. As seen on Fig. 9, there is some systematic tendency for the second layer data to stay below our first layer results.

It is interesting to study from a theoretical point of view these two-dimensional systems which exist as Fermi fluids in a much wider range of densities than the bulk system. Presently there are several microscopic theories trying to explain Fermi-liquid behavior in liquid ^{3}He. The almost localized fermion model[25,26] treats liquid ^{3}He as almost localized and explains the susceptibility enhancement by an according enhancement of the effective mass. This model leads to the expressions $m^*/m = (1 - I^2)^{-1}$ and $F_0^a = -p[1 - (1 + I)^{-2}]$ where I is the normalized on-site interaction potential $I = U/U_c$ and p is a quantity that depends mainly on the density of states and can be taken to be approximately one for a symmetric band.[26] Taking $p = 1$ and substituting for the normalized interaction potential I, one obtains the expression

$$1 + F_0^a = \frac{1}{(1 + \sqrt{1 - m/m^*})^2},$$

which is shown by the hatched line in Fig. 9.

The paramagnon model[27,28] explains the susceptibility enhancement as being due to spin fluctuations and the high-density system as being almost ferromagnetic. The calculation in two dimensions leads to the expressions[28] $\chi/\chi_0 = (1 - \bar{I})^{-1}$ and $m^*/m = 1 + \frac{9}{2}\bar{I}\ln\{1 + \bar{p}_1^2\bar{I}[12(1 - \bar{I})]^{-1}\}$, where $\bar{I}$ is the normalized interaction potential and $\bar{p}_1 = p_1/p_F$ is the momentum cutoff value which is of order 1.[28] Again taking $\bar{p}_1 = 1$ and substituting for the normalized interaction potential $\bar{I}$, one obtains the expression

$$\frac{m^*}{m} = 1 + \frac{9}{2}\left(1 - \frac{\chi_0}{\chi}\right)\ln\left(1 + \frac{1 - \chi_0/\chi}{12\chi_0/\chi}\right),$$

from which the dependence of the Landau parameter F_0^a on the inverse of the effective mass can be deduced easily. This dependence is shown by the point-hatched line in Fig. 9. Note that we are considering here the crudest approximation of both theories which, in addition, are not supposed to apply to the whole density range. The paramagnon model is only applicable for large effective masses, since only the most divergent terms in $(1 - \bar{I})^{-1}$ have been considered in the calculation.[29] It is not known presently whether the necessary corrections for smaller interactions are important. A similar restriction holds for the almost localized fermion theory which in addition is only valid for a large number of next neighbor atoms.[26] Therefore, its predictions are to be taken with care when

comparing to 2D data. The theories are therefore valid for roughly $m^*/m > 3$, whereas the range accessible to experiment is $m^*/m < 5$ and $\chi/\chi_0 < 20$. It is therefore rather surprising that both theories describe particularly well the experimental data in a large density range. It should be noted that the trend of our data is coherent with the value $1 + F_0^a = 0.25$ given by the phenomenological "spin-glass" model by Castaing[30] which is valid in the limit of large effective masses. As seen in Fig. 9, all data on 2D and 3D ^{3}He correspond to a high-density regime where the Landau parameter F_0^a is not strongly dependent on the effective mass. In such a regime characterized by strong correlations it is not obvious that a Fermi-liquid theory does indeed apply. Recent microscopic calculations by Bouchaud and Lhuillier[31] suggest a strong dimerization of the ^{3}He atoms and the disappearance of the Fermi surface. In order to investigate the crossover (or eventually the transition?) from the correlated regime to the weakly interacting Fermi fluid, it would be interesting to extend the measurements to lower densities. This would require a substantial improvement of the experimental techniques.

It has been implicitly assumed in this article that the fluid phase is homogeneous. Although recent theoretical calculations[32] suggest that the fluid may be unstable at low temperatures, giving rise to a liquid-gas coexistence, experimental evidence favors a homogeneous system at submonolayer coverages; phase separation, however, is not ruled out by the experiments at multilayer coverages.[33]

V. CONCLUSION

Although the ground state of adsorbed ^{3}He at low submonolayer coverages is a liquid, heterogeneity leads to the localization of a fraction of the adsorbed atoms, identified by their large NMR susceptibility at low temperatures. A linear coverage dependence of the localized fraction has been experimentally determined; it agrees qualitatively with a model based on a distribution of binding energies.[14]

The onset of commensurate solid-liquid coexistence has been observed at a coverage 0.0449 atoms/Å^2. This border of the ^{3}He/graphite phase diagram agrees well with

heat capacity data,[6] but disagrees with previous NMR measurements.[7] Corrections for heterogeneity lead to estimate the liquid density at this coverage to be 0.0434 atoms/Å^2 which would be the onset value for a perfect graphite substrate. This result should be helpful for establishing precise quantum Monte Carlo calculations. A small shift of Greywall and Busch's coverage scale, in fact already considered as an alternative in the analysis of the heat capacity measurements, leads to a simple and consistent picture of the submonolayer structural phase diagram. The existence of a vacancy solid in a large density range is ruled out by our data.

The nuclear susceptibility of submonolayer liquid ^{3}He is rather well described by phenomenological expressions for two-dimensional Fermi fluids. The effective Fermi temperatures could be determined in a large density range, including within the commensurate solid-liquid coexistence regime. The susceptibility enhancement factor is found to be very similar, at the same density, to that determined for liquid ^{3}He adsorbed on a ^{4}He preplated graphite sample,[19] suggesting that substrate corrugation and the strength of the adsorption potential do not affect strongly the Fermi-liquid behavior. A similar conclusion is reached when discussing the Landau parameter F_0^a determined in both systems. The comparison requires the effective mass values determined by heat capacity;[21] we found it necessary to correct their presently known coverage dependence using our data for the submonolayer films.

A comparison of our experimental results on the first layer liquid to the almost localized fermion model shows a good agreement as already found by Lusher et al.[19] for the second layer. However, we show that a similar agreement can be claimed with the paramagnon model and also with the spin-glass model. It is surprising that theories with very different physical basis yield essentially the same results. We hope that the present results will motivate the extension to the low-density range of the calculations performed a decade ago for bulk ^{3}He.

From the experimental point of view, it would be desirable to perform measurements on liquid ^{3}He systems at lower densities. This would require higher sensitivity in the NMR detection, but also a simultaneous determination of the heat capacity on the same sample, to suppress coverage scale errors.

[1] Grafoil is manufactured by Union Carbide.

[2] H. Godfrin, R.E. Rapp, and H.J. Lauter, Physica B 169, 177 (1991).

[3] D.S. Greywall, Physica B 197, 1 (1994).

[4] H. Godfrin and R.E. Rapp, Adv. Phys. (to be published).

[5] J. Saunders, C.P. Lusher, and B.P. Cowan, in Excitations in Two-Dimensional and Three-Dimensional Quantum Fluids, edited by by A.G.F. Wyatt and H. Lauter (Plenum Press, New York, 1991).

[6] D.S. Greywall and P.A. Busch, Phys. Rev. Lett. 65, 2788 (1990).

[7] J. Saunders, C.P. Lusher, and B.P. Cowan, Phys. Rev. Lett. 64, 2523 (1990).

[8] R.E. Rapp and H. Godfrin, Phys. Rev. B 47, 12004 (1993).

[9] D.S. Greywall and P.A. Busch, J. Low Temp. Phys. 46, 451 (1981).

[10] M. Bretz, J.G. Dash, D.C. Hickernell, E.O. McLean, and O.E. Vilches, Phys. Rev. A 8, 1589 (1973).

[11] A. Abragam, Principles of Nuclear Magnetism (Oxford University Press, New York, 1961).

[12] Extensive and detailed results exist for mixture films: See D.T. Sprague, N. Alikacem, P.A. Sheldon, and R.B. Hallock, Phys. Rev. Lett. 72, 384 (1994), and references therein.

[13] A.M. Dyugaev, Sov. Sci. Rev. A Phys. **14**, 1 (1990).

[14] R.L. Elgin, J.M. Greif, and D.L. Goodstein, Phys. Rev. Lett. **41**, 1723 (1978); R.L. Elgin and D.L. Goodstein, Phys. Rev. A **9**, 2657 (1974).

[15] M.W. Cole, D.R. Frankl, and D.L. Goodstein, Rev. Mod. Phys. **53**, 199 (1981).

[16] B.P. Cowan and A.J. Kent, Phys. Lett. **106A**, 54 (1984).

[17] R.A. Guyer, Phys. Rev. Lett. **39**, 1091 (1977).

[18] D.C. Hickernell, E.O. McLean, and O.E. Vilches, Phys. Rev. Lett. **28**, 789 (1972).

[19] C.P. Lusher, B.P. Cowan, and J. Saunders, Phys. Rev. Lett. **67**, 2497 (1991).

[20] E.O. McLean, Ph.D. thesis, University of Washington, 1972.

[21] D.S. Greywall and P.A. Busch, Phys. Rev. Lett. **65**, 64 (1990).

[22] Tabulated values in D. Vollhardt and P. Wölfle, *The Superfluid Phases of ^3He* (Taylor & Francis, London, 1990), p. 31.

[23] D.S. Greywall, Phys. Rev. B **41**, 1842 (1990).

[24] H.J. Lauter, H. Godfrin, V.L.P. Frank, and H.P. Schild-berg, Physica B **165&166**, 597 (1980).

[25] W.F. Brinkmann and T.M. Rice, Phys. Rev. B 2, 4302 (1970); P.W. Anderson and W.F. Brinkmann, in *The Physics of Liquid and Solid Helium*, edited by K.H. Bennemann and J.B. Ketterson (Wiley, New York, 1978).

[26] D. Vollhardt, Rev. Mod. Phys. **56**, 99 (1984).

[27] S. Doniach and S. Engelsberg, Phys. Rev. Lett. **17**, 433 (1966); N.F. Berk and J.R. Schrieffer, *ibid.* **17**, 750 (1966); M.T. Béal-Monod, S.K. Ma, and D.R. Fredkin, *ibid.* **20**, 929 (1968).

[28] M.T. Béal-Monod and A. Theumann, in *Ordering in Two Dimensions*, edited by S.K. Sinha (Elsevier, New York, 1980).

[29] M.T. Béal-Monod (private communication).

[30] B. Castaing, J. Phys. (France) Lett. **41**, L333 (1980).

[31] J.P. Bouchaud and C. Lhuillier, Z. Phys. B **75**, 283 (1989).

[32] B. Brami, F. Joly, and C. Lhuillier, J. Low Temp. Phys. **94**, 63 (1994).

[33] H. Godfrin, R.E. Rapp, K.-D. Morhard, J. Bossy, and Ch. Bäuerle, Phys. Rev. B **49**, 12377 (1994).